Original papers

Med Ultrason 2024, Vol. 26, no. 2, 138-146
DOI: 10.11152/mu-4329

A radiomics model based on transrectal ultrasound for predicting prostate cancer

Yanhua Huang[1*], Hongwei Qian[2,3*], Yuanyuan Zheng[1], Huiming Song[1], Xiatian Liu[1]

** the authors share the first authorship*

[1]Department of Ultrasound, Shaoxing People's Hospital, [2]Department of Hepatobiliary and Pancreatic Surgery, Shaoxing People's Hospital, [3]Shaoxing Key Laboratory of Minimally Invasive Abdominal Surgery and Precise Treatment of Tumor, Shaoxing, China

Abstract

Aim: Prostate cancer (PCa) is one of the most common neoplasms in men. However, the value of ultrasound-based radiomics for diagnosing PCa remains uncertain. **Material and methods:** We retrospectively analyzed ultrasonic and clinical data from 373 patients. Patients were divided into two groups according to the pathological results. Radiomics features were extracted from TRUS, and we screened the optimal features to construct radiomics models. Relationships between clinical characteristics and prostate lesions were identified by univariate and multivariate logistic regression analysis. Finally, a clinical-radiomics model was developed, and then visualized in the form of a nomogram. **Results:** Of the 373 patients, 178 had benign disease and 195 had malignant disease. The support vector machine (SVM) classification model showed the best performance, while the diagnostic performance of the clinical model was poorer than that of the radiomics model ($p<0.05$) or the combined (clinical-radiomics) model ($p<0.05$). In general, the combined model demonstrated the highest AUC and proved to be more advantageous. **Conclusion:** The prediction model we constructed based on TRUS predicted PCa preoperatively with high efficiency. In addition, combining radiomics with clinical factors improved diagnostic accuracy.

Keywords: prostate cancer; transrectal ultrasound; radiomics; machine learning; image segmentation

Introduction

Prostate cancer (PCa) is a prevalent malignancy affecting the prostate, characterized as an epithelial cancer. It ranks among the most frequently diagnosed cancers in males [1]. In recent years, the worldwide incidence of PCa has shown annual increases, especially in relatively developed regions [2].

PCa diagnosis relies mainly on serum prostate-specific antigen (PSA) measurement, digital rectal examination, and prostate biopsy. However, PSA values can be influenced by a variety of factors, including prostatitis and urinary tract infections. Digital rectal examination is also a limited physical examination method, with a positive detection rate of only 41% [3]. At present, the gold standard for diagnosing and distinguishing benign and malignant prostate lesions before surgery is prostate biopsy. Nonetheless, the biopsy is an invasive procedure with a particular risk of complications, including the possible spread of tumor cells along the needle path [4]. Furthermore, owing to the heterogeneity of tumors, pathological diagnosis via puncture biopsy potentially risks misdiagnosis and over- or under-treatment [5]. Thus, it is essential to acknowledge the limitations and potential complications associated with biopsy, despite it being the gold standard for diagnosing PCa. Given these challenges, the focus of our paper is not to discover an alternative diagnostic method, which would indeed be challenging. Instead, our aim is to enhance the quality of imaging diagnosis prior to biopsy procedures. In doing so, we strive to address the existing problem in diagnosing and distinguishing benign and malignant prostate lesions.

Received 21.07.2023 Accepted 04.01.2023
Med Ultrason
2024, Vol. 26, No 2, 138-146
Corresponding author: Xiatian Liu
Shaoxing People's Hospital, 568 Zhongxing North Road, Shaoxing 312000, China
E-mail: lxtsxsrmyy@163.com
Phone: +86-575-88558627

Nowadays, the application of multiparametric magnetic resonance imaging (mpMRI) and the prostate imaging reporting and data system (PI-RADS) has made the imaging diagnosis of PCa more systematized and normalized [6]. A previous study has stated that the combination of magnetic resonance imaging/ultrasound fusion-targeted biopsy and systematic biopsy can enhance the detection rate of PCa [7]. Moreover, pre-biopsy mpMRI was recommended in the 2021 American Urological Association, National Comprehensive Cancer Network, and European Association of Urology guidelines. Nonetheless, although mpMRI and PI-RADS play a vital role in the diagnosis and evaluation of PCa, some limitations remain regarding their clinical application. For example, the use of mpMRI is limited by high cost, restricted availability, and long examination times, while PI-RADS relies on the operator's clinical experience and has the disadvantage of a long learning curve [8]. Another major limitation of PI-RADS is high inter-reader variability, which affects cancer detection [9].

Transrectal ultrasound (TRUS) is another standard imaging method for assessing PCa. This method is frequently used as it combines the advantages of being economical, convenient, real-time, and straightforward to perform [10]. With the application of contrast-enhanced ultrasound (CEUS) and shear wave elastography (SWE), TRUS has also been demonstrated to be highly reliable for the assessment of PCa. However, reliance on the visual elements produced by TRUS means a large number of image features representing tumor heterogeneity may potentially be overlooked, leading to lower diagnostic accuracy, compared with biopsy [10]. Furthermore, the accuracy of TRUS as a diagnostic technique is highly reliant on the expertise and experience of the operator, making it heavily operator-dependent. This dependence on the operator's skill level can lead to reduced reproducibility and potentially impact the reliability of the results.

Radiomics, a method of extracting tumor-related features from medical images, was first proposed by Lambin in 2012 [11]. In recent years, radiomics has gained widespread application in the field of cancer diagnosis and differential diagnosis, as well as the evaluation of clinical stage, outcome, and metastasis of tumors. Its use involves extracting a large number of quantitative features from medical images, which are then analyzed and correlated with specific cancer types or characteristics. This emerging approach has shown great promise in enhancing the accuracy and precision of cancer diagnosis, aiding in the distinction between various cancer subtypes, and providing valuable insights for personalized treatment strategies. In contrast to TRUS, which displays limitations in terms of the repeatability and representativeness of quantitative outcomes, radiomics can lead to enhanced objectivity and reproducibility through the quantitative analysis of the extracted features. Previous studies [12,13] have demonstrated that radiomics is highly reliable at differentiating malignant from benign prostate tissue. However, these studies were mainly based on magnetic resonance imaging (MRI) [14, 15].

Despite the advantages of TRUS, PCa lesions are very obscure or even invisible on ultrasound images. Thus, radiomics based on TRUS has rarely been performed because of the difficulty in outlining regions of interest (ROIs). To overcome these difficulties and facilitate the performance of radiomics based on TRUS, we aimed to develop a more accessible and convenient ROI delineation method. Furthermore, our ultimate goal was to create and validate a prediction model utilizing TRUS for distinguishing between benign and malignant prostate lesions. By leveraging TRUS data and combining it with other relevant clinical and radiomic features, we aimed to establish a robust and accurate predictive tool that can aid in the early detection and differentiation of prostate cancer from benign conditions.

Material and methods

Patients

Our institutional ethics committee reviewed and approved this study. We retrospectively analyzed the ultrasound and clinical data of 460 patients who underwent prostatic needle biopsy in our hospital from September 2019 to August 2022. The inclusion criteria were: (1) TRUS was performed within the two-week period preceding the biopsy; (2) patients complained of clinical symptoms (urinary frequency, urinary urgency, dysuria) or showed increased PSA levels; (3) PCa or benign prostate conditions were pathologically proven after biopsy. The exclusion criteria were: (1) incomplete pathological data (n=41); (2) incomplete clinical data (n=12); (3) previous treatment before biopsy (n=6); (4) ultrasound images were lacking or image quality was suboptimal (n=28). Finally, 373 patients were enrolled in the study, including 178 patients with benign lesions and 195 patients with malignant lesions (Table I). The patients were randomly allocated into two groups: a training group consisting of 261 individuals and a validation group consisting of 112 individuals. The division was done in a 7:3 ratio, ensuring that both groups were representative and suitable for conducting further investigations and analyses.

A flowchart of the included and excluded patients is shown in figure 1.

Image acquisition

All patients were examined using a color Doppler ultrasound (Esaote, MyLabTMTwice, Italy) equipped with a 3-13 MHz transrectal dual-plane probe (TRT33). The studies were performed with patients lying in a knee-thorax position and breathing quietly. Images showing the prostate tissues at their widest point (maximum diameter) were saved as digital imaging and communications in medicine (DICOM) format files for further analysis.

Biopsy procedure

The "12+X" biopsy, a targeted biopsy based on a 12-core transrectal systematic biopsy, was performed on all patients. A 12-core systematic biopsy entails the insertion of a needle into specific regions of the prostate based on a predefined template. These regions include the medial and lateral apex, medial and lateral mid-prostate, and medial and lateral base in both lobes of the prostate. The biopsy procedure involves sampling from each of these 12 designated regions for diagnostic purposes [16,17]. In addition, one or two extra needles were used to further biopsy the suspicious area.

Image segmentation

ROI segmentation was carried out using ITK-SNAP software (Version 3.8.0, www.itksnap.org) to manually outline the edge of the prostate tissues in images showing the widest point of the prostate. This procedure was performed independently by two experienced sonographers blind to patients' clinical data (fig 2). ROI segmentation was repeated one week later.

Feature extraction and dimension reduction

For feature extraction, we employed an open-source Python package called Pyradiomics. Pyradiomics is specifically designed for extracting a wide range of radiomic features from medical images. To extract as much information as possible from the ultrasound images, we applied wavelet, LoG, square, square-root, logarithm, exponential, and gradient filters. The extracted features were divided into three categories: first-order features, shape features, and texture features. As the features differed by several orders of magnitude, the features were then scaled using standard Z-score scaling.

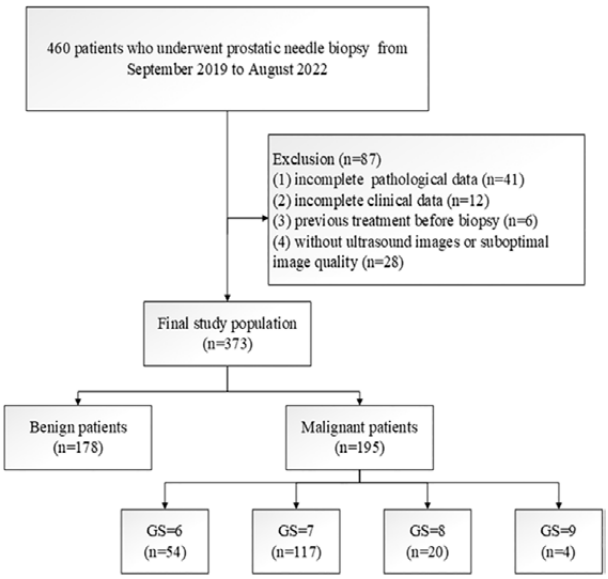

Fig 1. Flowchart of included and excluded patients.

Intra- and inter-class coefficients (ICC) were used to assess the reproducibility of all radiomics features. Intra-class coefficients were calculated by comparing the features extracted by different sonographers, and inter-class coefficients were calculated by comparing features extracted at different times (one week apart). In our study, features with an ICC value greater than 0.8 were considered to be reproducible. The ICC is a statistical measure used to assess the agreement or reproducibility of measurements between different raters or measurements taken at different times. A higher ICC value indicates a greater level of agreement or reproducibility between measurements. By setting a threshold of 0.8 for the ICC, we en-

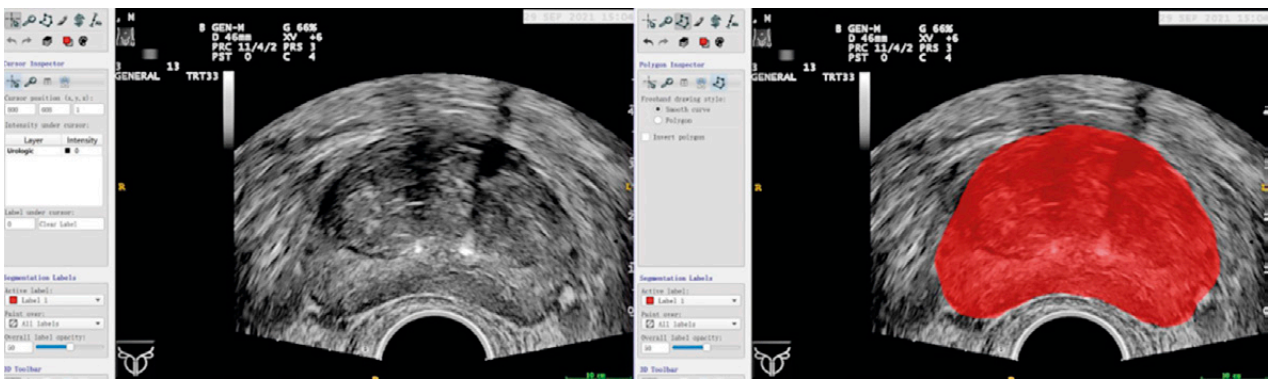

Fig 2. An example of region of interest (ROI) delineation on transrectal ultrasound (TRUS) imaging in ITK-SNAP software.

sured that only features with a high level of consistency and reproducibility in our study were included in the analysis. This step helps to minimize potential variability in the results and enhances the reliability of the features selected for further investigation or model development.

We employed three methods to screen the selected features: the Variance method, t-test, and the Least Absolute Shrinkage and Selection Operator (LASSO). By combining these screening methods, we aimed to identify a set of robust and informative radiomic features for the development of our prediction model.

Model construction and evaluation

We constructed several radiomics models using different modelling methods. To assess the performance of each model, we conducted receiver operating characteristic (ROC) curve analysis and calculated the corresponding area under the curve (AUC). Associations between clinical characteristics and prostate lesions were identified by univariate and multivariate logistic regression analysis. A clinical-radiomics model, combining radiomics features and clinical risk factors, was created through multivariate logistic regression and represented in a nomogram.

Statistical analysis

All radiomics procedures and statistical analyses were performed using Python software (Version 3.8.5). For constructing the nomogram, R language (Version 4.2.2, R Foundation for Statistical Computing, Vienna, Austria) was utilized. Continuous variables were presented as either mean±standard deviation or median and range, based on the normality of their distribution. The comparison of continuous variables was conducted using either the t-test or Mann-Whitney U test, depending on the data distribution. To evaluate the differences between different models, we employed the Delong test. Decision curve analysis (DCA) was performed to assess the clinical usefulness of the models. A significance level of $p<0.05$ was considered statistically significant for all analyses.

Results

Patient characteristics

In the study, a total of 373 patients were ultimately included and randomly divided into two groups: the training group with 261 patients and the validation group with 112 patients. The details about age, serum total prostate-specific antigen (tPSA), serum free prostate-specific antigen (fPSA), f/t PSA, prostate volume (PV), and prostate-specific antigen density (PSAD) and Gleason score are shown in Table I. PV was calculated using the formula: PV = anteroposterior diameter × vertical diameter × transverse diameter × 0.52. PSAD was calculated as the ratio of total PSA to PV (PSAD = tPSA / PV).

Radiomics model

Feature extraction from both the original and filtered images resulted in 1595 features. All features had inter-class correlation coefficients >0.80, and 1549/1595 features had intra-class correlation coefficients >0.80. Radiomic features were found to exhibit a high degree of correlation, which was visualized using a heatmap (fig 3). Therefore, dimensionality reduction was crucial for building a parsimonious model.

We deleted low variance radiomics features (close to 0) and removed features correlating with any other feature with an absolute Pearson correlation >0.9. Following further dimension reduction using LASSO regression, we obtained eleven radiomics features (fig 4).

The selected features and their coefficient values are shown in Table II.

To determine the best modelling method for model construction after selecting the features, we tested various methods, including support vector machine (SVM), random forest (RF), K nearest neighbor (KNN), logistic regression (LR), and artificial neural network (ANN). The SVM model showed the best diagnostic performance, with an AUC value of 0.809 (0.727–0.891) in the validation group. In the same group, the AUC was 0.792 (0.706–0.877) for the RF model, 0.733 (0.638–0.827) for the KNN model, 0.769 (0.68-0.858) for the LR model, and 0.763 (0.673–0.853) for the ANN model. Compari-

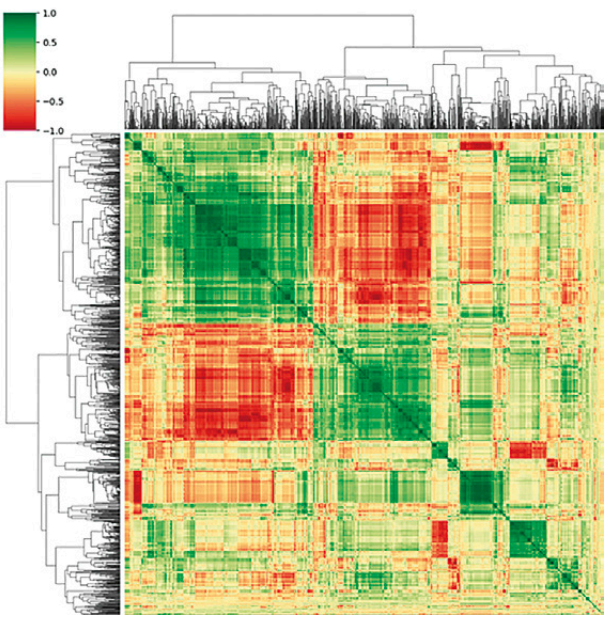

Fig 3. Correlation heatmap demonstrating the high degree of correlation between radiomics features.

sons of performance across the different classifiers are shown in fig 5.

For a more detailed assessment of the SVM prediction model, we calculated a radiomics score (Radscore) for each patient (fig 6). The results demonstrated the ability of the SVM-based Radscore to discriminate PCa from benign prostate diseases.

Clinical model

We conducted both univariate and multivariate logistic regression analyses to identify significant clinical factors for predicting PCa. In the univariate analysis, each clinical factor was evaluated individually to assess its association with PCa. Factors that showed a statistically significant relationship with PCa in the univariate analysis were further considered in the multivariate analysis (Table III).

The factors that remained statistically significant in the multivariate analysis were considered as significant predictors of PCa. In our study, multivariate logistic regression analysis identified age, f/t PSA, and PV as independent predictors for PCa, with $p<0.05$. A logistic

Table I. Demographic and clinical characteristics of patients

Variables	**Benign**	**Malignant**	**p**	**Training Group**		**p**	**Validation Group**		**p**
				Benign	**Malignant**		**Benign**	**Malignant**	
	(n=178)	**(n=195)**		**(n=130)**	**(n=131)**		**(n=48)**	**(n =64)**	
Age (year)	70.00 (65.00-74.50)	73.00 (69.00-77.00)	<0.01	69.0 (64.0-74.0)	72.0 (69.0-76.0)	<0.01	70.08±7.63	72.84±6.47	0.043
Serum tPSA (ng/ml)	8.72 (5.66-12.67)	11.01 (7.42-22.51)	<0.01	9.09 (5.53-12.44)	11.45 (7.43-24.93)	0.004	10.29±7.42	21.09 ± 50.4	0.147
Serum fPSA (ng/ml)	2.04±1.95	3.10±9.17	0.13	2.01±1.93	2.96±7.07	0.143	2.12±2.02	3.38±12.41	0.492
f/t PSA	0.17 (0.13-0.25)	0.11 (0.08-0.17)	<0.01	0.17 (0.12-0.24)	0.11 (0.08-0.17)	<0.01	0.21±0.1	0.15±0.13	0.006
PV(ml)	46.66 (33.96-67.789)	34.90 (26.02-49.75)	<0.01	45.92 (33.62-66.06)	37.86 (27.53-50.89	<0.01	49.56 (39.22-69.44)	33.16 (23.46-43.5)	<0.01
PSAD (ng/ml/ml)	0.18(0.11-0.27)	0.32 (0.18-0.74)	<0.01	0.19 (0.11-0.27)	0.33 (0.16-0.71)	<0.01	0.17 (0.1-0.24)	0.3 (0.19-0.77)	0.007
Gleason score									
6		n=54			n=36			n=18	
7		n=117			n=79			n=38	
8		n=20			n=13			n=7	
9		n=4			n=3			n=1	

tPSA, total prostate-specific antigen; fPSA, free prostate-specific antigen; PV, prostate volume; PSAD, prostate-specific antigen density

Table II. The selected features and their coefficient values

Filter	**Feature class**	**Feature**	**Coefficient**
wavelet-LLH	glszm	LargeAreaLowGrayLevelEmphasis	-0.07161
wavelet-LHL	firstorder	Mean	0.038097
wavelet-LHL	ngtdm	Busyness	-0.010299
wavelet-HLH	glcm	Imc1	-0.056328
wavelet-HLH	gldm	SmallDependenceEmphasis	-0.011672
wavelet-HLH	gldm	SmallDependenceHighGrayLevelEmphasis	-0.006664
wavelet-HHH	glszm	ZonePercentage	0.014305
wavelet-LLL	ngtdm	Strength	0.017343
square	ngtdm	Busyness	-0.018506
gradient	glszm	SizeZoneNonUniformity	-0.018586
lbp-2D	firstorder	InterquartileRange	-0.006282

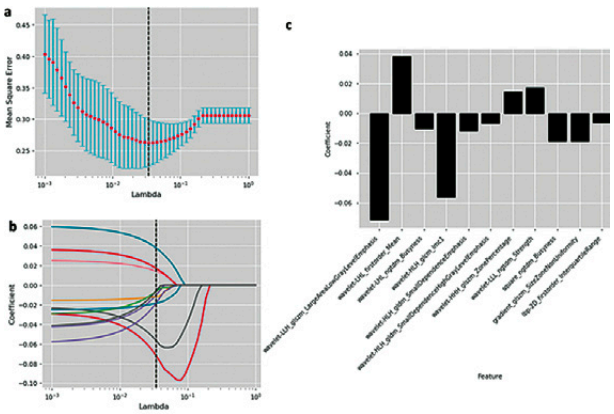

Fig 4. (a, b) Least absolute shrinkage and selection operator (LASSO) regression complexity was controlled using a tuning parameter lambda; the optimal lambda value for the minimized mean squared error was 0.03393221771895328. (c) The eleven selected variables and their coefficient values are shown.

model based on the independent predictors was then established, yielding an AUC of 0.776 (0.721–0.832) in the training group and 0.742 (0.649–0.835) in the validation group (fig 7). Diagnostic efficacy was significantly different (p=0.002) in the radiomics and clinical models.

Combined model

Next, we integrated the independent predictors with the Radscore values to build a combined model, which is presented as a nomogram (fig 8).

The combined model showed an enhanced ability to discriminate PCa from benign prostate diseases, with an AUC greater than that of either the radiomics model or the clinical model (fig 9a). In addition, according to the Delong test, the combined model achieved significantly better diagnostic efficacy than the clinical model (p=0.003), but not the radiomics model (p=0.729), indicating the reliability of radiomics in predicting PCa. Afterward, we employed DCA to evaluate the clinical utility of all three models (as shown in fig 9b). For each model, the area under the decision curve was found to be higher than the "treat all" strategy (represented by the solid grey line) or the "treat none" strategy (represented by the dotted grey line). This indicates that our models offer superior net benefits compared to treating all patients or treating none at all. The DCA results demonstrate the potential clinical usefulness and added value of our predictive models in guiding treatment decisions for patients with PCa. Among the three prediction models, the combined model stood out with the largest area under the decision curve and demonstrated the most significant benefit across a wide range of threshold probabilities. This finding indicates that the combined model, which

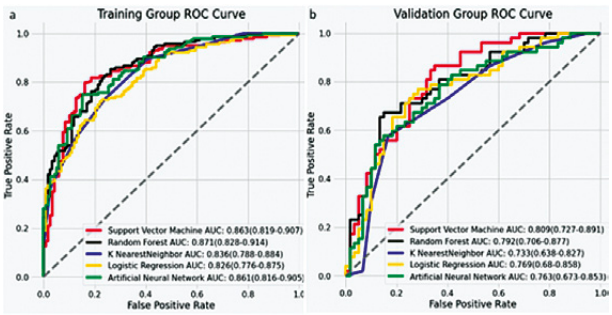

Fig 5. Receiver operating characteristic curve analysis of the modelling methods. The SVM model showed the best diagnostic performance, with AUC values of 0.863 (0.819–0.907) in the training group (a) and 0.809 (0.727–0.891) in the validation group (b).

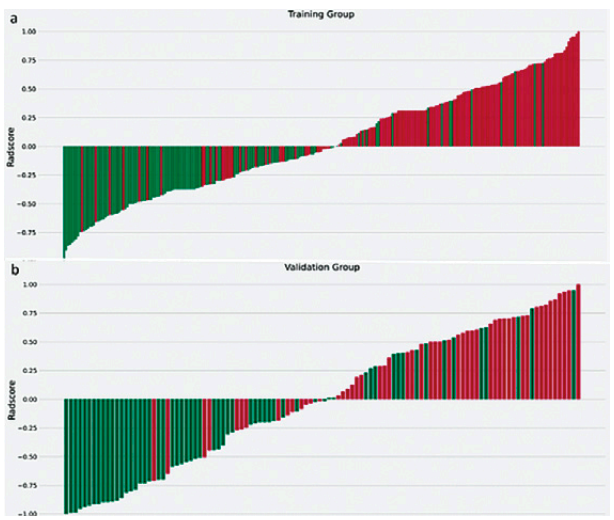

Fig 6. The histograms show the normalized Radscore values for benign (green) and malignant (red) prostate disease cases in the training group (a) and validation group (b).

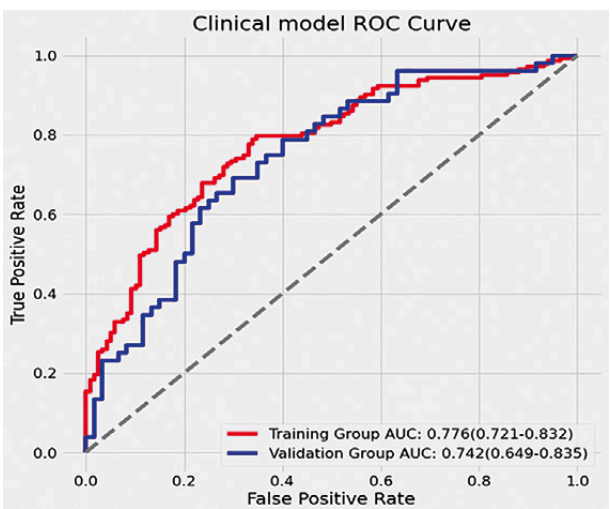

Fig 7. Receiver operating characteristic curve analysis of the clinical model.

Table III. Univariate and multivariate logistic analysis of clinical factors.

Variables	Univariate logistic analysis		Multivariate logistic analysis	
	OR (95% CI)	p-value	OR (95% CI)	p-value
Age(year)	1.065(0.031-1.103)	<0.001	1.074(1.037-1.115)	<0.001
Serum tPSA(ng/ml)	1.033(1.013-1.057)	0.003		0.65
Serum fPSA(ng/ml)	1.046(0.990-1.136)	0.185		
f/t PSA	0.003(0-0.044)	<0.001	0.011(0-0.202)	0.004
PV (ml)	0.977(0.965-0.988)	<0.001	0.984(0.968-0.998)	0.033
PSAD (ng/ml/ml)	8.439(3.380-25.337)	<0.001		0.103

tPSA, total prostate-specific antigen; fPSA, free prostate-specific antigen; PV, prostate volume; PSAD, prostate-specific antigen density

integrated radiomics features and clinical risk factors, outperformed the other models in terms of predictive accuracy and clinical utility. Its superior performance suggests that the combined model has the potential to be more effective in assisting clinicians in making informed decisions for the differentiation of PCa.

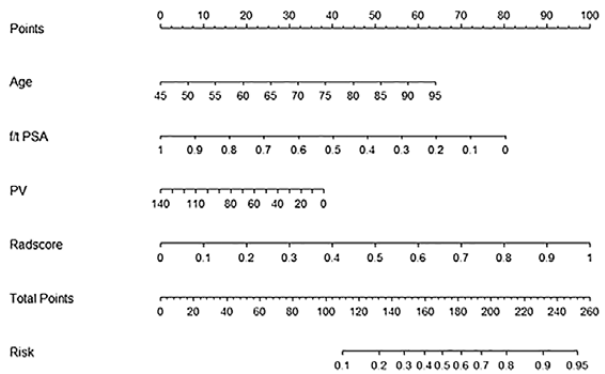

Fig 8. Nomogram of the combined model for predicting PCa.

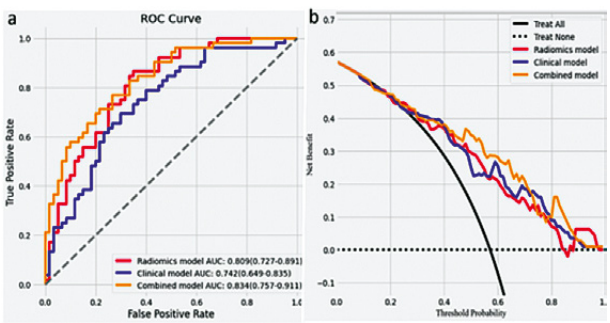

Fig 9. (a) Comparison of receiver operating characteristic curves for differentiation of the radiomics, clinical, and combined models. (b) Decision curves for the radiomics, clinical, and combined models.

Discussion

To the best of our knowledge, this is the first radiomics model based on a single ultrasound mode (B-mode) to enable discrimination between malignant and benign prostate lesions without requiring cooperation with SWE, CEUS, or MRI. Diagnostic value was high for all the predictive models constructed using various methods, including SVM, RF, KNN, LR, and ANN.

Of the various modelling methods we tested, the SVM model displayed the best diagnostic performance when used on the validation group. SVM is a classic machine learning method based on rigorous statistics theory and is particularly suitable for small samples with good robustness [18]. Fleury et al [19] employed five distinct methods for constructing a radiomics model to differentiate between benign and malignant breast lesions. Among these methods, the SVM (Support Vector Machine) model exhibited the highest accuracy, achieving an AUC value of 0.84.

Many studies [12-14,20-22] have also used radiomics methods to differentiate prostate cancer from benign prostate lesions, and the reliability of radiomics based on MRI has been proven. However, radiomics studies based on ultrasound are rare. In a study conducted by Wildeboer et al [23] they reported that a multiparametric classifier, which combined B-mode, SWE, and CEUS, achieved an AUC of 0.75 for PCa and 0.9 for significant PCa. Liang et al [17] reported a clinical-radiomics combined model with an AUC value of 0.90 for PCa.

The main reason for the lack of radiomics studies using TRUS is the difficulty of delineating prostate cancer lesions in TRUS images, as PCa lesions are very obscure and even invisible (in most cases) to the naked eye. In previous TRUS-based radiomics studies, lesion boundaries could only be drawn after combining the results of B-Mode ultrasound, SWE, CEUS, and biopsy; thus, the ROI delineation process was extremely complex. However, the ROI delineation method in our study was very different. Several studies have suggested that changes in prostate tissues, such as tumor cell infiltration and connective tissue reactions [24-26], occur before the morphological changes detectable by MRI or TRUS are visible to the naked eye; thus, it may be possible to diagnose and evaluate PCa by analyzing these invisible changes. However,

few studies have examined this possibility. To capture the greatest amount of information possible, we chose the maximum cross-section of the prostate as the ROI and used radiomics to analyze the tissue changes. The results of our study demonstrated that, with the use of radiomics, the changes produced by tumor cell infiltration and connective tissue reactions in prostate tissue had a diagnostic value for PCa. Furthermore, the new method we employed for the ROI delineation process was highly reliable.

Radiomics features can be classified into first-order features, second-order features, and high-order features. First-order features, or histogram features, indicate the grey-level values of individual voxels without reflecting spatial relationships or correlations. Second-order features, also known as texture analysis, pertain to the characterization of spatial relationships among voxels with similar gray levels within a lesion [27], which also reflect tumor heterogeneity and complexity [28,29]. High-order features involve applying filters to images [15] to obtain more unobservable information from the original images [30]. In contrast to computer tomography (CT) or MRI images, grey-scale ultrasound images are two-dimensional, which means that they contain less information than CT or MRI images. To extract the maximum information from the ultrasound images, we used several filters (wavelet, LoG, square, square-root, logarithm, exponential, and gradient) and obtained a total of eleven radiomics features, eight of which were wavelet features. The wavelet filter enables images to be further divided into sub-images with different frequency components, facilitating the exploration of spatial heterogeneity within ROIs at multiple scales [31]. Our findings indicated the crucial role of the wavelet filter in predicting pathological results, consistent with previous studies [31,32].

In our study, univariate and multivariate logistic analysis identified age, f/t PSA, and PV as significant clinical factors for predicting PCa. The clinical model, which relied on the selected clinical risk factors, demonstrated a satisfactory ability to differentiate between malignant and benign prostate lesions. However, it did not achieve the same level of performance as either the radiomics model or the combined model. Both the radiomics model and the combined model, which integrated radiomics features and clinical risk factors, outperformed the clinical model in terms of predictive accuracy and discrimination ability. This finding highlights the added value of incorporating radiomics features into the predictive models, as they contribute to a more robust and accurate differentiation of prostate lesions compared to using clinical risk factors alone. Nonetheless, DCA demonstrated the capacity of clinical factors to improve diagnostic ability as supplemental data in the combined model.

Despite the satisfactory performance of the prediction model, our study had some limitations. First, single-center data was used for the radiomics modelling, whereas multi-center prospective studies may have greater variability in image acquisition and protocols, which could improve the generalization ability of the model [13]. Second, ROI analysis was not performed on a particular region of the tumor but on the cross-section of the prostate. As tumors may not necessarily always lie within this specific area, cancer lesions in other planes could sometimes be missed. Thus, although our ROI delineation method was much more convenient than other, more complex methods and yielded satisfactory results, we assume that prostate cross-sections specifically including the tumor focus may enhance model accuracy. Third, this was a retrospective study, which may introduce potential selective bias. Finally, we did not use genomic data, immunohistochemistry, or local pathologic analysis in the prediction model.

Conclusion

Inconclusion, we have presented a new ROI delineation method, which did not require the precise location of the prostate lesions for analysis. Furthermore, we developed a combined radiomics-clinical model using TRUS, which exhibited high levels of accuracy in discriminating between benign and malignant prostate lesions. The model's accuracy and generalizability made it effective in distinguishing between these two types of lesions. Our model reduces unnecessary biopsies by accurately identifying non-cancerous lesions, allowing patients to avoid costly and risky procedures. Additionally, it aids in early cancer detection, increasing the chances of a successful treatment, which enhances healthcare cost-efficiency and patient comfort. The incorporation of both radiomics features and clinical risk factors in the model contributed to its enhanced performance, providing clinicians with a reliable and valuable tool for improving the diagnosis and management of prostate lesions.

Acknowledgment: The work was sponsored by Shaoxing Medical Key Discipline (2019SZD05). The funders did not influence the analysis or publication.

Conflict of interest: none

References

1. Siegel RL, Miller KD, Jemal A. Cancer statistics, 2018. CA Cancer J Clin 2018;68:7-30.
2. Mottet N, Bellmunt J, Bolla M, et al. EAU-ESTRO-SIOG Guidelines on Prostate Cancer. Part 1: Screening, Diagno-

sis, and Local Treatment with Curative Intent. Eur Urol 2017;71:618-629.
3. Heidenreich A, Bastian PJ, Bellmunt J, et al. EAU guidelines on prostate cancer. part 1: screening, diagnosis, and local treatment with curative intent-update 2013. Eur Urol 2014;65:124-137.
4. Loeb S, Vellekoop A, Ahmed HU, et al. Systematic review of complications of prostate biopsy. Eur Urol 2013;64:876-892.
5. Ukimura O, Coleman JA, de la Taille A, et al. Contemporary role of systematic prostate biopsies: indications, techniques, and implications for patient care. Eur Urol 2013;63:214-230.
6. Turkbey B, Rosenkrantz AB, Haider MA, et al. Prostate Imaging Reporting and Data System Version 2.1: 2019 Update of Prostate Imaging Reporting and Data System Version 2. Eur Urol 2019;76:340-351.
7. Cauni VM, Stanescu D, Tanase F, Mihai B, Persu C. Magnetic resonance/ultrasound fusion targeted biopsy of the prostate can be improved by adding systematic biopsy. Med Ultrason 2021;23:277-282.
8. Smith CP, Harmon SA, Barrett T, et al. Intra- and inter-reader reproducibility of PI-RADSv2: A multireader study. J Magn Reson Imaging 2019;49:1694-1703.
9. Wajswol E, Winoker JS, Anastos H, et al. A cohort of transperineal electromagnetically tracked magnetic resonance imaging/ultrasonography fusion-guided biopsy: assessing the impact of inter-reader variability on cancer detection. BJU Int 2020;125:531-540.
10. van Hove A, Savoie PH, Maurin C, et al. Comparison of image-guided targeted biopsies versus systematic randomized biopsies in the detection of prostate cancer: a systematic literature review of well-designed studies. World J Urol 2014;32:847-858.
11. Lambin P, Rios-Velazquez E, Leijenaar R, et al. Radiomics: extracting more information from medical images using advanced feature analysis. Eur J Cancer 2012;48:441-446.
12. Liu B, Cheng J, Guo DJ, et al. Prediction of prostate cancer aggressiveness with a combination of radiomics and machine learning-based analysis of dynamic contrast-enhanced MRI. Clin Radiol 2019;74:896.e891-e896.e898.
13. Ji X, Zhang J, Shi W, et al. Bi-parametric magnetic resonance imaging based radiomics for the identification of benign and malignant prostate lesions: cross-vendor validation. Phys Eng Sci Med 2021;44:745-754.
14. Ginsburg SB, Algohary A, Pahwa S, et al. Radiomic features for prostate cancer detection on MRI differ between the transition and peripheral zones: Preliminary findings from a multi-institutional study. Magnetic Reson Imaging 2017;46:184-193.
15. Gillies RJ, Kinahan PE, Hricak H. Radiomics: Images Are More than Pictures, They Are Data. Radiology 2016;278: 563-577.
16. Borkowetz A, Platzek I, Toma M, et al. Comparison of systematic transrectal biopsy to transperineal magnetic resonance imaging/ultrasound-fusion biopsy for the diagnosis of prostate cancer. BJU Int 2015;116:873-879.
17. Liang L, Zhi X, Sun Y, et al. A Nomogram Based on a Multiparametric Ultrasound Radiomics Model for Discrimination Between Malignant and Benign Prostate Lesions. Front Oncol 2021;11:610785.
18. Yip SSF, Aerts HJWL. Applications and limitations of radiomics. Phys Med Biol 2016;61:R150-R166.
19. Fleury E, Marcomini K. Performance of machine learning software to classify breast lesions using BI-RADS radiomic features on ultrasound images. Eur Radiol Exp 2019;3:34.
20. Cameron A, Khalvati F, Haider MA, Wong A. MAPS: A Quantitative Radiomics Approach for Prostate Cancer Detection. IEEE Trans Biomed Eng 2016;63:1145-1156.
21. Xu M, Fang M, Zou J, et al. Using biparametric MRI radiomics signature to differentiate between benign and malignant prostate lesions. Eur J Radiol 2019;114:38-44.
22. Chen T, Li M, Gu Y, et al. Prostate Cancer Differentiation and Aggressiveness: Assessment With a Radiomic-Based Model vs. PI-RADS v2. J Magn Reson Imaging 2019;49:875-884.
23. Wildeboer RR, Mannaerts CK, van Sloun RJG, et al. Automated multiparametric localization of prostate cancer based on B-mode, shear-wave elastography, and contrast-enhanced ultrasound radiomics. Eur Radiol 2020;30:806-815.
24. Harvey H, Morgan V, Fromageau J, O'Shea T, Bamber J, deSouza NM. Ultrasound Shear Wave Elastography of the Normal Prostate: Interobserver Reproducibility and Comparison with Functional Magnetic Resonance Tissue Characteristics. Ultrason Imaging 2018;40:158-170.
25. Xiang LH, Fang Y, Wan J, et al. Shear-wave elastography: role in clinically significant prostate cancer with false-negative magnetic resonance imaging. Eur Radiol 2019;29:6682-6689.
26. Good DW, Stewart GD, Hammer S, et al. Elasticity as a biomarker for prostate cancer: a systematic review. BJU Int 2014;113:523-534.
27. Incoronato M, Aiello M, Infante T, et al. Radiogenomic Analysis of Oncological Data: A Technical Survey. Int J Mol Sci 2017;18:805.
28. Li Z, Mao Y, Huang W, et al. Texture-based classification of different single liver lesion based on SPAIR T2W MRI images. BMC Med Imaging 2017;17:42.
29. Han Y, Wang W, Yang Y, et al. Amide Proton Transfer Imaging in Predicting Isocitrate Dehydrogenase 1 Mutation Status of Grade II/III Gliomas Based on Support Vector Machine. Front Neurosci 2020;14:144.
30. Zwanenburg A, Vallières M, Abdalah MA, et al. The Image Biomarker Standardization Initiative: Standardized Quantitative Radiomics for High-Throughput Image-based Phenotyping. Radiology 2020;295:328-338.
31. Wu S, Zheng J, Li Y, et al. A Radiomics Nomogram for the Preoperative Prediction of Lymph Node Metastasis in Bladder Cancer. Clin Cancer Res 2017;23:6904-6911.
32. Xu L, Yang P, Liang W, et al. A radiomics approach based on support vector machine using MR images for preoperative lymph node status evaluation in intrahepatic cholangiocarcinoma. Theranostics 2019;9:5374-5385.